Proceedings of the ASME 2018 International Design Engineering Technical Conferences and Computers and Information in Engineering Conference
IDETC2018
August 26-29, 2018, Quebec City, Quebec, Canada

DETC2018-86149

ANALYSIS AND DIMENSIONAL SYNTHESIS OF A ROBOTIC HAND BASED ON THE STEWART-GOUGH PLATFORM

Connor M. McCann
Yale University
Department of Mechanical Engineering
New Haven, Connecticut, USA
connor.mccann@yale.edu

Aaron M. Dollar
Yale University
Department of Mechanical Engineering
New Haven, Connecticut, USA
aaron.dollar@yale.edu

ABSTRACT

In this paper, we study the dimensional synthesis of a Stewart-Gough platform-inspired dexterous robotic hand, seeking to optimize the hand's geometric design parameters to achieve the largest possible 6-degree-of-freedom workspace of a grasped object serving in the place of the "platform." We present an analysis of the hand mechanism that considers both object stability from frictional contact forces as well as kinematic motion transmissibility, seeking a balance between these two properties. We examine the effect of variations in the kinematic and frictional parameters on both the workspace size of the hand as well as on the motion quality throughout the workspace across a range of grasped object sizes. We then present a spectrum of optimal designs that weight these two performance criteria differently. Most notably, the palm radius of the hand was found to have the greatest effect on the workspace size, with smaller palms exhibiting significantly larger workspaces. Overall, this work serves to inform the design process for dexterous robotic hands based on this common kinematic configuration, with the ultimate goal of increasing the dexterity of robotic manipulators to facilitate more versatile interactions with the environment.

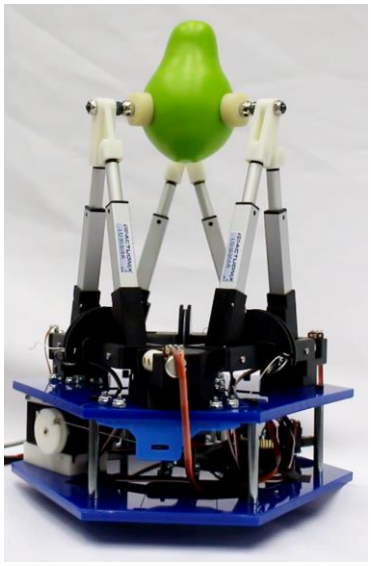

Fig. 1. Experimental prototype of the Stewart-Gough platform-inspired robotic hand, pictured here grasping an artificial pear.

INTRODUCTION

For many robotic manipulation tasks, it is advantageous to not only grasp objects, but also to manipulate them within the grasp of a robotic hand. This type of within-hand dexterity has previously been shown to improve positioning accuracy, increase efficiency, and allow a manipulator to avoid obstacles and singular configurations through kinematic redundancy [1]. Traditionally, dexterous robotic hands that are capable of such within-hand manipulation have been modeled after the human hand, resulting in highly complicated systems that require extensive actuation/sensing and precise control schemes [2], [3].

An alternative to this anthropomorphic approach is to draw inspiration from parallel robots, given their high dexterity and mechanical simplicity. In our previous work, we proposed a novel hand design based on the Stewart-Gough platform that effectively transferred these desirable properties from the realm of parallel robotics into a dexterous hand framework [4]. This hand consisted of six prismatic joints arranged into three fingers (Fig. 1) that collectively formed a parallel mechanism structure when grasping an object (where the object serves as the platform of the mechanism and the fingers as the legs). In initial experiments, this hand performed very well, demonstrating 6-degree-of-freedom (DOF) manipulation capabilities over a large workspace.

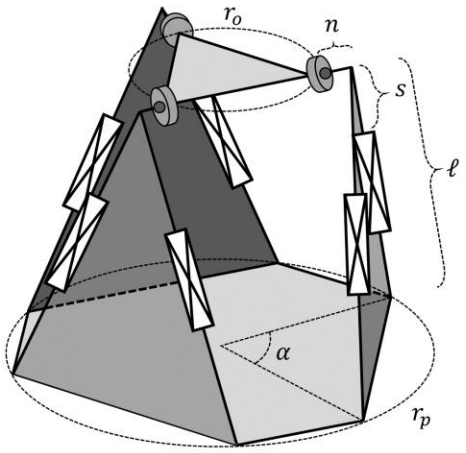

Fig. 2. Kinematic structure of the hand, showing the dimensional design parameters. Each finger consists of two prismatic actuators connected in parallel.

One drawback of parallel mechanisms is that their performance can be greatly impacted by their geometric design parameters [5], [6]. Therefore, it is critical to optimize these parameter values to achieve the greatest possible performance—a process referred to as dimensional synthesis. Much work has previously been devoted to the dimensional synthesis of traditional Stewart-Gough platforms, seeking to optimize a variety of performance metrics such as workspace size, precision, and dynamic behavior [7]–[9]. While the results of these studies are informative, they cannot be directly applied to the proposed hand design, since traditional Stewart-Gough platforms lack the frictional contact constraints present at the hand's fingertips. Thus, a more detailed analysis is necessary.

In this work, we seek to model the behavior of the proposed Stewart-Gough hand design and to examine the effect of varying the mechanism's design parameters on the 6-DOF workspace size and motion quality across the workspace, as measured through the Local Transmission Index (LTI) [10]. We begin with a description of the mechanism architecture and derive the force equilibrium constraints that must be satisfied to maintain frictional stability at the fingertips. We then formulate a design optimization to maximize the 6-DOF workspace size while ensuring effective motion transmission through the resulting parallel mechanism structure. Finally, we present the results of this optimization and examine the effects of the hand's various design parameters on its performance.

MECHANISM DESCRIPTION

The mechanism analyzed in this paper consists of three fingers, each comprised of two universal-prismatic-spherical (UPS) kinematic chains connected in parallel such that their spherical joints are coincident (Fig. 2). A compliant fingerpad is mounted at the spherical joint with a magnetic ball/socket connection and serves to facilitate reliable contact with the object. In addition to the six prismatic joints, which are actuated, a single revolute "grasp actuator" (not pictured in Fig. 2 but visible in the bottom left of Fig. 1) is included beneath the palm of the hand, which serves to close the fingers inward on the object. This actuator is operated in torque control and is connected by an underactuated tendon differential to the three fingers, ensuring that they all receive equal, inward torque toward the object regardless of its position/orientation. Further information about the design of this hand can be found in [4].

TABLE 1: DESIGN PARAMETERS OF THE HAND.

Symbol	Quantity	Non-Dimensional Form
ℓ	extended actuator length	1
r_p	palm radius	r_p/ℓ
r_o	object radius	r_o/ℓ
s	actuator stroke length	s/ℓ
n	spherical joint normal offset	n/ℓ
α	finger base angle	α
τ_g	grasp actuator torque	1
μ	finger friction coefficient	μ

In order to reduce the dimensionality of the design space and to ensure a symmetric workspace, all fingers are considered to be identical, symmetric about their own midplane, and equally spaced around the palm. Similarly, for simplicity, we restrict the current analysis to triangularly-symmetric objects (such as equilateral triangles and circles) with the fingertips spaced equally around the object's perimeter. By enforcing these constraints, a given design configuration of the hand/object system can be uniquely specified with eight parameters, as shown in Table I.

The first six parameters pertain to the spatial dimensions of the manipulator (depicted graphically in Fig. 2). Within each finger, the length of the UPS legs can be specified with the extended actuator length, ℓ, and the stroke length, s. (Note that in real-world linear actuators such as lead screws, $s \leq \frac{1}{2}\ell$, due to practical constraints on the frames of the actuators.) In the initial hand prototype presented in [4], the spherical joint at the end of each finger was offset from the plane of the actuators by a normal distance n. This was partially due to practical fabrication constraints, but also has the added benefit of increasing the clearance between the object and the finger. The geometry of the palm of the hand is specified with the palm radius, r_p, and the base angle of the fingers, α. Finally, the radius of the object, r_o, is also an important consideration, and it is generally desirable to maximize the manipulation capabilities over a range of object sizes for a general-purpose hand.

In addition to the spatial dimensions of the hand, the final two design parameters pertain to the forces exerted on the object. The grasping torque, τ_g, acting at the base of each finger, determines the magnitude of the contact forces exerted by the hand (and, therefore, the magnitude of wrenches that can be resisted). Additionally, the contact friction coefficient, μ, at the fingertips determines how easily the object will slip.

To ensure scale-invariant results, all length parameters were normalized to the extended actuator length, ℓ, and all force

values were taken with respect to the grasping torque, τ_g, both of which were set equal to unity. This choice of non-dimensionalizing parameters is a natural one, since these two quantities are determined by the choice of actuators being used in a prototype, but others could be chosen with only a resulting scaling of the actual results.

GRASP ANALYSIS

Kinematics

In order to determine whether a given 6-DOF object pose is feasible for a given hand design configuration, two main constraints must be satisfied. First, the pose must be kinematically feasible given the geometry of the mechanism. This criterion can be easily checked through the inverse kinematics of the hand that were derived previously in [4] by treating the hand-object system as an equivalent, traditional Stewart platform. If the desired pose requires an actuator length less than $\ell - s$ or greater than ℓ, then the pose is infeasible.

Slipping

The second constraint that the desired pose must satisfy is stability under slipping. This constraint involves the force balance at the fingertips of the hand, and therefore requires more detailed consideration. In order to model the contact forces of the hand, a point contact with friction model is adopted, with each fingertip being capable of exerting three independent wrench components—a normal force and two tangential frictional forces.

In adopting the formalism presented in [11], two coordinate frames, O and P, are located at the object center-of-mass and the center of the palm, respectively. Likewise, local contact coordinate frames, C_i, are situated at the contact sites with their z-axes directed along the inward surface normal of the object. To relate a vector, f_c, of the nine local contact wrench components (three per finger) expressed in the C_i frames to the net 6-DOF wrench, F_{net}, exerted on the object in the O frame, a 6×9 grasp matrix, $\mathbf{G}$, is defined such that $\mathbf{G}f_c = F_{\text{net}}$. For the grasp to be in static equilibrium, F_{net} must exactly counter the external wrench, F_e acting on the object, yielding:

$$\mathbf{G}f_c = -F_e \tag{1}$$

In order to determine whether a given object pose is stable with respect to slipping for a particular external wrench, it is necessary to solve this system for f_c. Unfortunately, $\mathbf{G}$ is rank-deficient and, therefore, the original system must be augmented with three additional equations to yield a unique solution. To derive these supplemental equations, the component of force normal to the plane of each finger is calculated. Since the grasp torque exerted at the base of the finger, τ_g, is constant and the moment arm of the finger is known for a given pose, this normal component of force can be found. To express this quantity, an additional coordinate frame, N_i, is introduced at the top of each finger with its z-axis directed along this normal direction toward the spherical joint (Fig. 3).

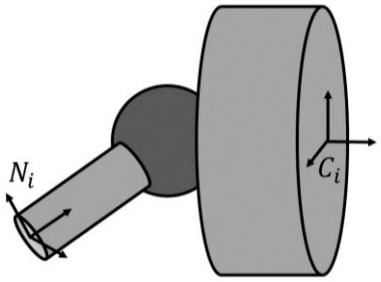

Fig. 3. Fingertip detail view showing the finger-normal and contact frames, N_i and C_i.

Thus, one of the six components of the contact wrench can be expressed in the N_i frame. This wrench can be related to the C_i frame through the adjoint transform matrix [11]:

$$F_{N_i} = \mathbf{Ad}^T_{g^{-1}_{N_i C_i}} F_{C_i} \tag{2}$$

The 6-dimensional F_{c_i} can then be related to the 9-dimensional f_c as:

$$F_{n_i} = \mathbf{Ad}^T_{g^{-1}_{N_i C_i}} \mathbf{Q}_i f_c \tag{3}$$

where:

$$\mathbf{Q}_1 \coloneqq [\mathbf{B} \quad \mathbf{0} \quad \mathbf{0}]$$
$$\mathbf{Q}_2 \coloneqq [\mathbf{0} \quad \mathbf{B} \quad \mathbf{0}]$$
$$\mathbf{Q}_3 \coloneqq [\mathbf{0} \quad \mathbf{0} \quad \mathbf{B}]$$
$$\mathbf{B} \coloneqq \begin{bmatrix} \mathbf{I}_{3\times 3} \\ \mathbf{0}_{3\times 3} \end{bmatrix}$$

Here the $\mathbf{Q}_i$ matrices simply serve to select the appropriate components from f_c, and $\mathbf{B}$ is the wrench basis for the point contact with friction model being used.

Finally, since only the normal force component of F_{N_i} is known, this component ($\tilde{F}_{N_i}$) is isolated as:

$$\tilde{F}_{N_i} = \mathbf{U}\,\mathbf{Ad}^T_{g^{-1}_{N_i C_i}} \mathbf{Q}_i f_c \coloneqq \tilde{\mathbf{G}}_i f_c \tag{4}$$

where:

$$\mathbf{U} = [0 \quad 0 \quad 1 \quad 0 \quad 0 \quad 0]$$

Thus, Eqn. 4 represents one additional equation per finger in terms of f_c that can be used to augment Eqn. 1. This augmented system (Eqn. 5) is now full rank and can be inverted to yield an expression for f_c (Eqn. 6):

$$\begin{bmatrix} \mathbf{G} \\ \tilde{\mathbf{G}}_1 \\ \tilde{\mathbf{G}}_2 \\ \tilde{\mathbf{G}}_3 \end{bmatrix} f_c = \begin{bmatrix} -F_e \\ \tilde{F}_{N_1} \\ \tilde{F}_{N_2} \\ \tilde{F}_{N_3} \end{bmatrix} \tag{5}$$

$$\boldsymbol{f_c} = \begin{bmatrix} \mathbf{G} \\ \tilde{\mathbf{G}}_1 \\ \tilde{\mathbf{G}}_2 \\ \tilde{\mathbf{G}}_3 \end{bmatrix}^{-1} \begin{bmatrix} -\boldsymbol{F_e} \\ \tilde{\boldsymbol{F}}_{N_1} \\ \tilde{\boldsymbol{F}}_{N_2} \\ \tilde{\boldsymbol{F}}_{N_3} \end{bmatrix} \tag{6}$$

Once the f_c vector has been computed, the minimum required friction coefficient, $\mu_{\min}$, can be found such that the

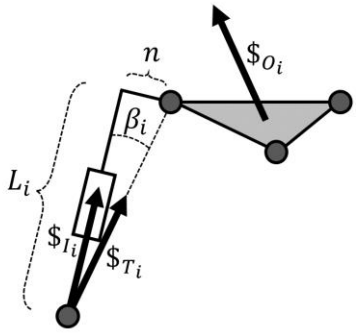

Fig. 4. Relevant unit screw axes for computation of the Local Transmission Index (LTI). Note that for clarity only the i^{th} leg is drawn. $\$_{I_i}$ is the input unit twist screw of the actuator, $\$_{T_i}$ is the unit wrench screw transmitted to the platform, and $\$_{O_i}$ is the output unit twist screw achieved by the platform with all other actuators locked and just actuating leg i.

total frictional force on each finger is less than or equal to $\mu_{\min}$ multiplied by the normal force. For any $\mu \geq \mu_{\min}$, the grasp will be stable, otherwise it will slip.

OPTIMIZATION FRAMEWORK

To achieve the greatest possible performance from this mechanism architecture, the dimensional parameters of the hand must be optimized to yield the largest stable 6-DOF workspace (given the frictional contact constraints). Such an optimization must strike a balance between workspace size and motion quality to ensure a manipulator that can successfully manipulate through a large range of 6-DOF poses.

Motion Quality Metric

If the frictional constraints are met at a given pose, the entire hand-object system may be treated as a parallel manipulator, since the contact points remain fixed in the object frame. A number of different local metrics have been previously proposed to assess the motion quality of such a parallel manipulator [12], [13]. We adopt the Local Transmission Index (LTI) proposed in [10], which uses reciprocal screw products to quantify how effectively the actuators and mechanism are being utilized to transmit motion/loads to the end effector.

The LTI metric is composed of two sub-metrics that are computed for each leg of the parallel mechanism. First, the effectiveness of the actuator at transmitting power through the leg is quantified. This input transmission index for the i^{th} leg of the mechanism, λ_i, is defined as:

$$\lambda_i = \frac{\left|\$_{T_i} \circ \$_{I_i}\right|}{\left|\$_{T_i} \circ \$_{I_i}\right|_{\max}} \tag{7}$$

where $\$_{I_i}$ is the unit twist screw along the axis of the i^{th} actuator and $\$_{T_i}$ is the unit wrench screw that is exerted by the i^{th} leg on the moving platform (Fig. 4). This ratio compares the instantaneous power transmission between these two screws to the maximum possible transmission if $\$_{I_i}$ were optimally aligned with $\$_{T_i}$. The denominator in Eqn. 7 was shown to be unity for UPS kinematic chains in [10]. The numerator of this expression can be expanded as $\left|\$_{T_i} \circ \$_{I_i}\right| = \left|\hat{v}_{I_i} \cdot \hat{f}_{T_i}\right| = |\cos\beta_i|$. Thus, the final expression for λ_i is simply:

$$\lambda_i = |\cos\beta_i| \tag{8}$$

The second sub-metric considered by the transmission index assesses the effectiveness of power transmission from each leg to the output motion of the platform. This output transmission index for the i^{th} leg of the mechanism, η_i, is defined as:

$$\eta_i = \frac{\left|\$_{T_i} \circ \$_{O_i}\right|}{\left|\$_{T_i} \circ \$_{O_i}\right|_{\max}} \tag{9}$$

where $\$_{O_i}$ is the unit twist of the platform when only the i^{th} actuator is moved (all others being locked). In other words, $\$_{O_i}$ is the twist direction that is reciprocal to the constraints imposed by the five other legs. The denominator of Eqn. 9 can be expanded as follows, as demonstrated in [10]:

$$\left|\$_{T_i} \circ \$_{O_i}\right|_{\max} = \sqrt{\left(h_{T_i} + h_{O_i}\right)^2 + d_{\max}^2} \tag{10}$$

where h_{T_i} and h_{O_i} are the pitches of the respective screws and $d_{\max}$ is the maximum possible normal distance between the two screw axes.

Each of these input/output transmission indices (λ_i, η_i) ranges in value between 0 and 1, with 0 corresponding to a singular configuration and 1 corresponding to ideal power transmission. Thus, in order to characterize the overall performance of the manipulator, the Local Transmission Index (LTI) is defined as the minimum input/output transmission index value among all of the legs:

$$\text{LTI} = \min(\eta_i, \lambda_i) \qquad i \in [1,6] \tag{11}$$

In this way, LTI can be used to weight each point in the workspace based on its quality. Using this weighting function, the overall quality, Q, of a particular design is calculated as:

$$Q = \sum_{\text{Workspace}} LTI \tag{12}$$

TABLE 2: OPTIMIZATION PARAMETER RANGES.

Symbol	Quantity	Non-Dimensionalized	Range	Steps
r_p	palm radius	r_p/ℓ	$[0.25, 0.75]$	10
s	actuator stroke length	s/ℓ	$[0.15, 0.5]$	10
n	spherical joint offset	n/ℓ	$[0, 0.2]$	10
α	finger base angle	α	$\left[\frac{\pi}{6}, \frac{\pi}{2}\right]$	10
r_o	object radius	r_o/ℓ	$[0.15, 0.5]$	4
F_w	object weight	$F_r\ell/\tau_g$	$[0.2, 0.9]$	4
μ	finger friction coefficient	μ	$[0.1, 0.5]$	10

Parameter Discretization

In order to explore the design space of the mechanism, it is necessary to discretize the various parameters and test the hand's performance for each configuration. The parameter ranges chosen are presented in Table 2 and evenly spaced divisions within these ranges were tested. Given that the extended actuator length and grasping torque have been normalized to be 1, the remaining design parameters that must be optimized are the palm radius (r_p), the actuator stroke length (s), the spherical joint

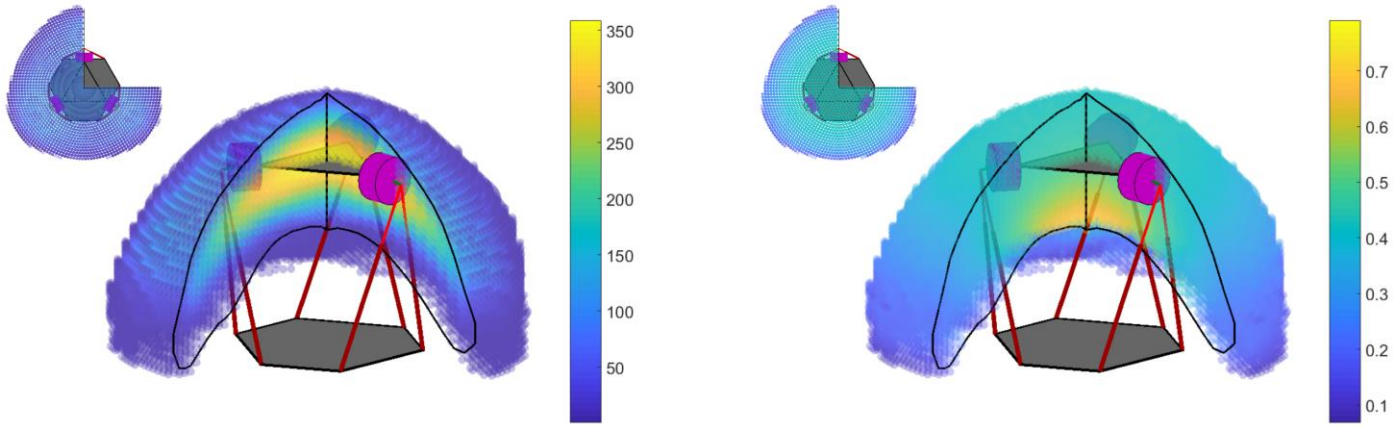

(a) (b)

Fig. 5. Workspace for the optimal hand design colored by (a) number of orientations achievable (out of 370 tested) at each position and (b) Local Transmission Index (LTI). One quadrant of the workspace has been cut away for clarity, with the black lines corresponding to the boundary of the cut region (the small top views also illustrate the cutaway region). These plots were generated with an object of radius $r_o/\ell = 0.27$, weight $F_w\ell/\tau_g = 0.43$, and friction coefficient $\mu = 0.5$.

normal offset distance (n), and the finger base angle (α). For each of these parameters, 10 values were tested, yielding a total of 10,000 designs that were considered.

When testing a particular hand design, the workspace was discretized into 170,145 positions and 370 spatial orientations, for a total of 62,953,650 total poses. At each pose, a number of different object properties were tested to gauge the design's average-case performance, including four object radii (r_o), four object weights (F_w), and 10 different friction coefficient values (μ).

In order to classify a particular pose as either "stable" or "unstable" given a set of object properties, we decided to mandate that the hand must be able to support the external force of the object's weight in arbitrary directions. Given that robotic hands are often mounted on arms (and therefore the direction of gravity in the hand's local coordinate frame is not known *a priori*), this requirement provides a measure of safety for any given grasp. In order to simulate this requirement, stability was checked for 41 different force application directions spaced approximately evenly around a sphere, and success was recorded only if all directions were found to be stable. If a pose was found to be successful, the LTI value for that pose was added to a running sum for Q (from Eqn. 12). In this way, the workspace size (weighted by the transmission index) could be calculated for each hand design.

RESULTS

Through this simulation, the quality value, Q, was calculated for each of the designs with every object radius, weight, and friction coefficient. To capture each design's average case performance, these Q values were then averaged over all of the object sizes and weights, yielding a single quality metric for each μ value. For a friction coefficient of 0.5, the optimal design parameters were found to be as follows, and the resulting hand and its workspace are plotted in Fig. 5.

$$\frac{r_p}{\ell} = 0.361 \qquad \alpha = 1.22$$
$$\frac{n}{\ell} = 0.044 \qquad \frac{s}{\ell} = 0.5$$

As can be seen in this plot, the hand's workspace is a large dome shape with a hollow interior, forming a shell around the hand. Qualitatively, this workspace appears to be significantly larger than those of most existing, serial-linkage hand designs, however, a formal comparison cannot be made due to a lack of quantitative workspace data for these other hand designs.

In Fig. 5a, the workspace is colored according to the number of orientations that can be achieved at a particular position. We can observe that the maximal reorientation capabilities are observed near the center of the translational workspace. This region corresponds to the actuators being approximately halfway extended, giving them the greatest ability to reconfigure in either direction to achieve large object reorientations.

Fig. 5b is colored to show the average LTI value at each position. Here, the greatest transmission index values are achieved close to the palm in the center of the workspace. In this region, the actuators are nearly fully retracted, meaning that each pair of actuators in a particular finger are as far from parallel to each other as possible. In this way, the actuators provide the least redundancy, and the overall manipulator is, therefore, furthest from being singular.

Effects of Palm Radius (r_p) and Finger Angle (α)

While the optimal performance can be achieved with the design parameters listed above, it may not always be possible to realize these parameter values given practical design considerations when building a real prototype. Thus, it is important to understand the effects of varying each of the design parameters about this optimal point. To investigate these effects,

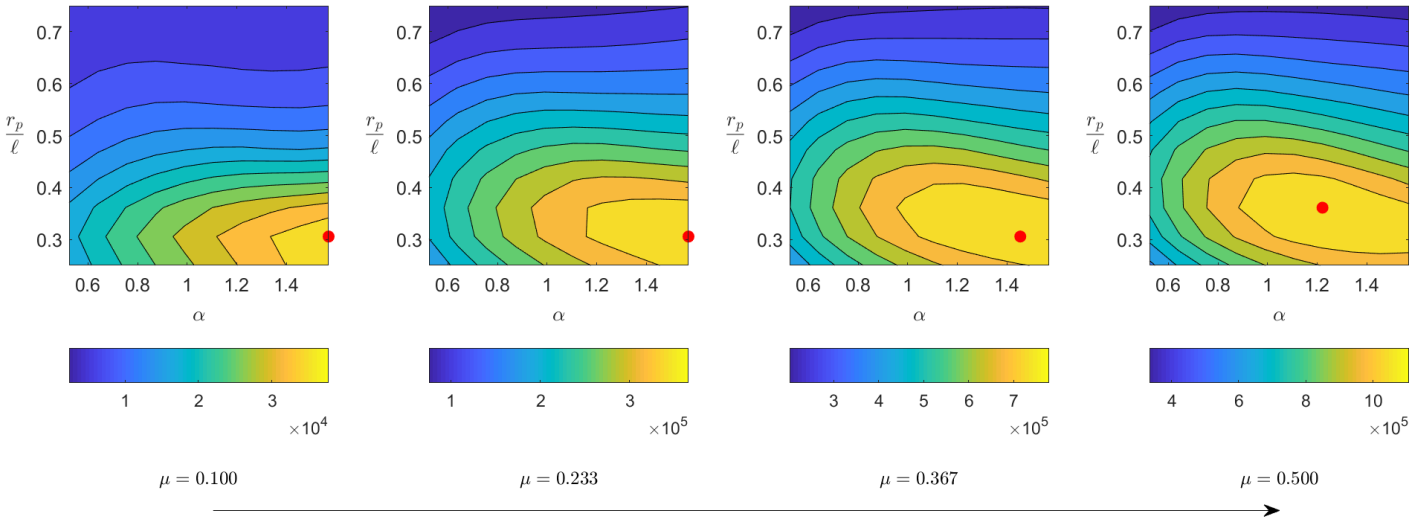

Fig. 6. Variation in workspace quality (Q) as a function of the main design parameters, r_p/ℓ and α. Within each plot, these two parameters were varied while the others were held at the optimal value. Each column corresponds to a different friction coefficient value.

Fig. 6 presents the variation in quality, Q, as the main design parameters, r_p/ℓ and α, are varied. In each contour plot, these two design parameters are varied while the other two (n/ℓ and s/ℓ) are held at the optimal values. Each plot corresponds to a different friction coefficient value.

From these plots, we see that the parameter that has the most impact on the hand's performance is the palm radius, since the quality metric falls off the most steeply as r_p is increased. Thus, when designing a hand with this configuration, the palm radius is the most important parameter to match to the optimal design.

Intuitively, it makes sense that the greatest performance would be achieved with small r_p values. As the palm decreases in size, the legs of the mechanism move closer together, and start to act almost like a single pivot point at the center of the palm, allowing the object to tip to the sides to form the shell-shaped workspace seen in Fig. 5. With larger palm radii, this tipping motion capability is reduced, and the object is limited to a much smaller region near the center of the workspace, and the lower portions of the optimal workspace become inaccessible.

Effects of spherical joint normal offset (n)

While the palm radius and finger angle are the most critical parameters for this hand design, it is also worthwhile to consider the spherical joint normal offset, n, as this value is often non-zero due to real-world fabrication constraints (such as with the prototype shown in Fig. 1). The effects of this design parameter are presented in Fig. 7, where n/ℓ is varied along with r_p/ℓ and α about the optimal point. In general, we observe that smaller values of n yield higher performance quality. This is likely because smaller n values result in $\$_{I_i}$ and $\$_{T_i}$ being more closely aligned in Fig. 4, resulting in higher input transmission index (λ_i) values for each leg.

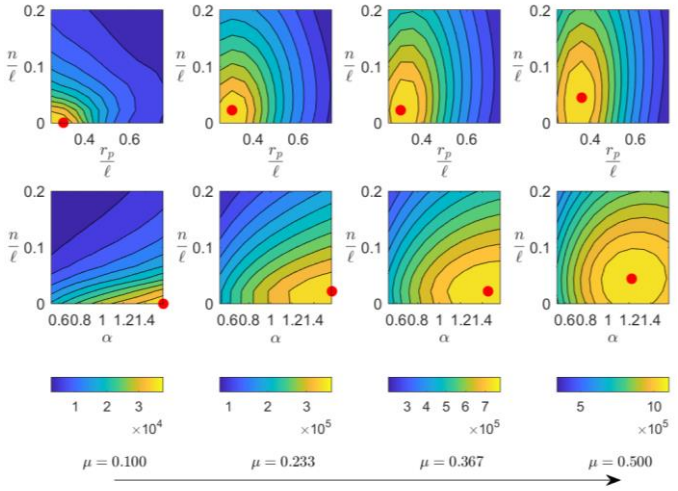

Fig. 7. Variation in workspace quality (Q) as a function of the spherical joint normal offset, n/ℓ. Within each plot, this parameter is varied along with either r_p/ℓ or α while the others were held at the optimal value. Each column corresponds to a different friction coefficient value.

Frictional Effects

In addition to all of the geometric design parameters, the contact friction coefficient, μ, plays a large role in determining the size of the hand's workspace. To illustrate these effects, the optimal design for a lower friction coefficient ($\mu = 0.28$) is plotted in Fig. 8 with the points that were kinematically feasible but failed due to slipping shown in red. Thus, these red points correspond to portions of the equivalent Stewart-Gough platform parallel mechanism's workspace that cannot be achieved with the hand.

There are three main loci of these inaccessible points, corresponding to gaps between each of the fingers. In these

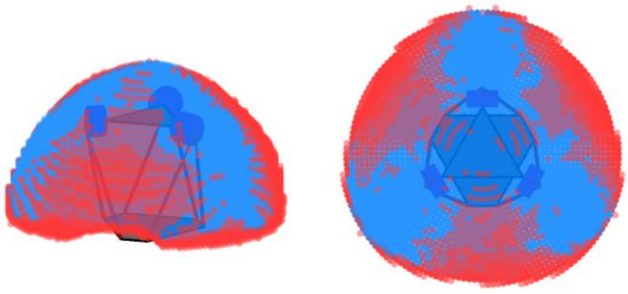

(a) (b)

Fig. 8. Visualization of slipping regions for the optimal design at $\mu = 0.28$. All points plotted in blue are achievable (for at least one orientation) given the frictional constraints, while all red points are unattainable due to slipping. (a) Oblique view. (b) Top view.

poses, one of the fingers effectively pushes the object between the other two, resulting in the ejection of the object. This kind of behavior was observed with the initial experimental prototype in [4], where the range of motion in these inter-finger directions was reduced compared to other directions. For larger μ values, the size of these loci is reduced, and the hand can achieve a greater percentage of the theoretical kinematic workspace.

In Fig. 6, we can observe that the optimal set of design parameters changes depending on the friction coefficient. In particular, with higher μ values, r_p and n tend to increase while α decreases. The upward trend in n can be explained by the fact that larger n values correspond to a longer effective finger length (since n is perpendicular to the linear actuator in each finger, as shown in Fig. 4, the effective finger length is the hypotenuse of the triangle formed by the two, $\ell_{\text{effective}} = \sqrt{\ell^2 + n^2}$). Thus, increasing n increases the reach of the fingers. For low μ values, this extra length is detrimental, since it increases the moment arm of the finger, meaning that the normal contact force will be smaller for a given grasp torque. With higher μ values, however, this slight decrease in normal force is acceptable, and the extra finger length can allow the hand to manipulate further.

A similar justification explains the trend toward decreasing α values as μ increases. For smaller α values, the width of the finger is reduced, allowing the linear actuators to get closer to being parallel (and, therefore, to reach further). This again has the disadvantage of reducing the contact force magnitude and thus is only advantageous for high μ values.

Another issue that arises from narrow fingers is that the linear actuators will become closer to singular, as they approach being parallel to each other. This would cause a decrease in the LTI values. This effect might explain the slight increase in r_p at the highest μ values. With a larger palm, the width of the fingers will increase for a given α value, helping to counteract this issue.

Global Transmission Index (GTI)

In addition to examining the Local Transmission Index, it is also possible to define the Global Transmission Index (GTI) as the average LTI value across the workspace of a manipulator:

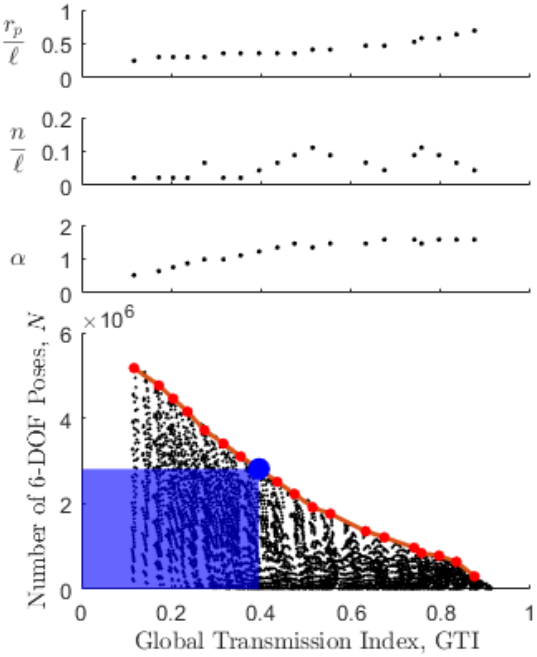

Fig. 9. Workspace size (i.e. number of 6-DOF poses) plotted against the Global Transmission Index (GTI) for $\mu = 0.5$. The points along the red line indicate optimal designs that can achieve the greatest workspace size for a particular GTI value. The variation of the design parameters along this line is plotted above. The blue point represents the design with the overall optimal Q value (i.e. the design plotted in Fig. 5).

$$\text{GTI} = \frac{Q}{N} \tag{13}$$

where N is the number of frictionally stable 6-DOF poses achieved. The GTI metric is thus normalized with respect to the workspace size (and therefore ranges between 0 and 1), so a high GTI score simply indicates consistently good transmission, regardless of the hand's workspace size. Such a metric may be appropriate where the actual size of the workspace is less important, such as precision positioning tasks, where accuracy is the main consideration.

To investigate this metric, Fig. 9 plots N vs GTI for all 10,000 designs considered (again at a μ value of 0.5). As is made clear in this plot, there is an approximately linear upper bound on the workspace size that can be achieved for a given GTI value. The points along this boundary—plotted in red—represent the optimal configurations of the hand for a given specified GTI value (i.e. the one with the largest workspace size), and the design plotted in blue corresponds to the overall optimal design identified in Fig. 5. Given the definition of GTI from Eqn. 13, we see that the quality Q corresponds to the rectangular area inscribed underneath a particular pose, and thus, the optimal design is situated mid-way along the line to maximize this area.

The corresponding design parameters for each of the optimal designs along the red line in Fig. 9 are plotted at the top of the figure. A few interesting trends can be observed here. First, as GTI increases, the optimal r_p value also increases. This matches with the trend previously discussed, where larger r_p values push the linear actuators further apart, resulting in a less

singular design for most poses. Conversely, a smaller r_p allows for a greater range of motion. For GTI values between approximately 0.5 and 1, the optimal α value was at the upper end of the range of values tested (near $\pi/2$), and only for low GTI values did it drop lower. Again, this comes down to a balance between range of motion and motion transmission. Finally, there is a slight upward tendency in n with GTI (for similar reasons), though this is less clear of a trend than with the other two variables.

CONCLUSIONS

In summary, a novel parallel mechanism-inspired dexterous robotic hand was analyzed to assess the effect of its design parameters on workspace size and force/motion transmission. An optimal hand design was found that exhibited a large range of motion with high motion transmission quality. Upon examining the effects of varying each of the design parameters about this optimal point, it was found that the palm radius has the largest effect on the reachable workspace size, with smaller palms achieving greater performance. Finally, a set of optimal designs was identified that each achieved the greatest workspace size for a given Global Transmission Index value, allowing one to make tradeoffs between workspace size and transmission quality depending on the particular application.

ACKNOWLEDGMENTS

The authors would like to thank Neil Bajaj, Jillian Cochran, and Walter Bircher for their assistance and consultation throughout this project.

REFERENCES

[1] R. R. Ma and A. M. Dollar, "On dexterity and dexterous manipulation," in *The Proceedings of the International Conference on Advanced Robotics (ICAR)*, 2011.

[2] A. Bicchi, "Hands for dexterous manipulation and robust grasping: a difficult road toward simplicity," *IEEE Trans. Robot. Autom.*, vol. 16, no. 6, pp. 652–662, 2000.

[3] C.-H. Xiong, W.-R. Chen, B.-Y. Sun, M.-J. Liu, S.-G. Yue, and W.-B. Chen, "Design and Implementation of an Anthropomorphic Hand for Replicating Human Grasping Functions," *IEEE Trans. Robot.*, vol. 32, no. 3, pp. 652–671, Jun. 2016.

[4] C. M. McCann and A. M. Dollar, "Design of a Stewart Platform-Inspired Dexterous Hand for 6-DOF Within-Hand Manipulation," in *Proceedings of the International Conference on Intelligent Robots and Systems (IROS)*, 2017, pp. 1158–1163.

[5] J. P. Merlet, *Parallel Mechanisms*, 2nd ed. Springer, 2006.

[6] R. Kelaiaia, A. Zaatri, O. Company, and L. Chikh, "Some investigations into the optimal dimensional synthesis of parallel robots," *Int. J. Adv. Manuf. Technol.*, vol. 83, no. 9–12, pp. 1525–1538, Apr. 2016.

[7] O. Masory and J. Wang, "Workspace evaluation of Stewart platforms," *Adv. Robot.*, vol. 9, no. 4, pp. 443–461, 1994.

[8] F. Jafari and J. E. McInroy, "Orthogonal gough-stewart platforms for micromanipulation," *IEEE Trans. Robot. Autom.*, vol. 19, no. 4, pp. 595–603, Aug. 2003.

[9] Z. Liu, X. Tang, Z. Shao, and L. Wang, "Dimensional optimization of the Stewart platform based on inertia decoupling characteristic," *Robotica*, vol. 34, no. 5, pp. 1151–1167, May 2016.

[10] J. Wang, C. Wu, and X.-J. Liu, "Performance evaluation of parallel manipulators: Motion/force transmissibility and its index," *Mech. Mach. Theory*, vol. 45, no. 10, pp. 1462–1476, Oct. 2010.

[11] R. M. Murray, Z. Li, and S. S. Sastry, *A Mathematical Introduction to Robotic Manipulation*. CRC Press, 1994.

[12] C. M. Gosselin, "Dexterity indices for planar and spatial robotic manipulators," in *Proceedings., IEEE International Conference on Robotics and Automation*, pp. 650–655.

[13] J. P. Merlet, "Jacobian, Manipulability, Condition Number, and Accuracy of Parallel Robots," *J. Mech. Des.*, vol. 128, no. 1, p. 199, Jan. 2006.